

# Noise-induced phase transitions in hybrid quantum circuits

Shuo Liu,<sup>1</sup> Ming-Rui Li,<sup>1</sup> Shi-Xin Zhang,<sup>2,\*</sup> Shao-Kai Jian,<sup>3,†</sup> and Hong Yao<sup>1,‡</sup>

<sup>1</sup>*Institute for Advanced Study, Tsinghua University, Beijing 100084, China*

<sup>2</sup>*Tencent Quantum Laboratory, Tencent, Shenzhen, Guangdong 518057, China*

<sup>3</sup>*Department of Physics and Engineering Physics,  
Tulane University, New Orleans, Louisiana, 70118, USA*

(Dated: January 31, 2024)

The presence of quantum noises inherent to real physical systems can strongly impact the physics in quantum hybrid circuits with local random unitaries and mid-circuit measurements. For example, an infinitesimal size-independent noise probability can lead to the disappearance of measurement-induced entanglement phase transition and the emergence of a single area-law phase. In this Letter, we investigate the effects of quantum noises with size-dependent probabilities  $q = p/L^\alpha$  where  $\alpha$  represents the scaling exponent. We have identified a noise-induced entanglement phase transition from a volume law to a power (area) law in the presence (absence) of measurements as  $p$  increases when  $\alpha = 1.0$ . With the help of an effective statistical model, we find that this transition is a first-order phase transition and shares the same analytical understanding as the noise-induced coding transition. We also discuss the differences between the effect of size-dependent noise and the boundary noise in the phase transitions. We validate our analytical predictions with extensive numerical results from stabilizer circuit simulations.

*Introduction.*— Measurement-induced phase transitions (MIPTs) have recently attracted significant attention and have been investigated in various setups [1–49]. These studies have revealed that the entanglement within a system undergoes a transition from a volume law to an area law as the probability of measurement increases. However, in real experimental systems, the presence of the environment unavoidably introduces quantum noises. The probability of these noises, which can be modeled by quantum channels, is denoted by  $q$ . In terms of the effective statistical model for MIPT, the quantum noises can be treated as symmetry-breaking fields that result in the disappearance of the entanglement phase transition and a single area-law entanglement phase [50–56]. This naturally raises the question: whether an entanglement phase transition is possible in the presence of quantum noises.

Previous research has investigated the MIPT from a power law phase to an area law phase in the presence of quantum noises at the spatial boundaries [57]. This can be regarded as a special case of quantum noises with size-dependent probabilities  $q = 2/L$ . Additionally, the effects of quantum noises in the bulk with size-dependent probabilities  $q = p/L$  have been explored in the context of a noise-induced computational complexity phase transition in random circuit sampling [58–60]. Therefore, it is important to investigate the phase diagram of MIPT with two tuning parameters: the probability of measurements and the size-dependent probability of quantum noises. The entanglement structures and critical behaviors associated with quantum noises of size-dependent probabilities, as well as the influence of other choices of scaling exponents  $\alpha$  in  $p/L^\alpha$  are also worth studying.

The entanglement structures and information protection are closely related [7, 8, 61–64]. From the perspective of information protection, a boundary noise-induced

coding transition occurs [65]. Below a finite critical probability of boundary noise, the encoded information can be protected after a hybrid evolution of time  $O(L)$ . However, if the probability of boundary noise exceeds this critical value, the information will be destroyed by the quantum noises. We expect that a similar noise-induced coding transition also exists in the presence of quantum noise in the bulk with  $q = p/L$ . Furthermore, a comprehensive theoretical understanding of the connections between noise-induced entanglement and coding transitions is needed.

In this Letter, we investigate the entanglement phase transition and coding transition in the presence of quantum noises with size-dependent probability, and give a more general phase diagram, Fig. 1 (c), for entanglement structures in the presence of both measurements  $p_m$  and noises  $q = p/L$ . While the dashed line represents the original MIPT,  $p_m = p_m^c$ , we identify a new noise-induced phase transition in the original volume law phase  $p_m < p_m^c$ , denoted by the solid line. This transition signifies that the system entanglement undergoes a transition from a volume law to a power law upon an increase in the noise probability. Building upon our previous works [55, 56], we attribute the power law entanglement to the Kardar-Parisi-Zhang (KPZ) fluctuation [57, 66–71] with an effective length scale  $L_{\text{eff}} \sim L/p$ . Besides, we have also investigated the coding transition in the presence of size-dependent quantum noises. The analytical picture of the coding transition is different from that presented in Ref. [65], where quantum noises are only applied on one spatial boundary. Theoretically, we have revealed that the noise-induced entanglement phase transition and coding transition can be understood within the same framework, giving the same critical properties. The transitions are of first-order with critical exponent  $\nu = 2.0$  [65]. To validate our theoretical findings, we have

conducted large-scale stabilizer circuit simulations, providing compelling evidence for the existence and universal behaviors of noise-induced entanglement phase transition and coding transition.

The choice of the scaling exponent  $\alpha$  for quantum noises is crucial for the noise-induced phase transitions. Previous studies focused on the disappearance of the entanglement phase transition in the presence of quantum noises [50–56], corresponding to  $\alpha = 0.0$ . In this Letter, we demonstrate that noise-induced phase transitions only occur at  $\alpha = 1.0$ . In terms of the effective statistical model, this is because only a single dominant spin configuration emerges for  $\alpha \neq 1$ . Without competition between different spin configurations, the noise-induced phase transitions disappear.

*Setup and observables.*— To investigate the noise-induced entanglement phase transition, we consider a one-dimensional system composed of  $L$   $d$ -qudits initially prepared in the state  $|0\rangle^{\otimes L}$ , as illustrated in Fig. 1 (a). At each discrete time step, a layer of random two-qudit unitary gates arranged in a brick-wall structure is applied. The projective measurements and quantum channels that characterize the quantum noises act on each qudit with probability  $p_m$  and  $q = p/L^\alpha$  respectively. To quantify the entanglement for the final mixed state [72, 73], we calculate the logarithmic entanglement negativity [74–83] between the left ( $A$ ) and right ( $B$ ) half chain of the final state

$$E_N = \log \|\rho^{T_B}\|_1, \quad (1)$$

where  $\rho^{T_B}$  is the partial transpose of  $\rho$  in subsystem  $B$  and  $\|\cdot\|_1$  is the trace norm. We also calculate the mutual information

$$I_{A:B} = S_A + S_B - S_{AB}, \quad (2)$$

where  $S$  is the entanglement entropy. Mutual information gives qualitatively similar scaling to  $E_N$  and provides a more intuitive understanding within the framework of the statistical model.

The setup for noise-induced coding transition is similar. The main difference is that one qudit of the system is maximally entangled with a reference qudit to encode one qudit quantum information into the system, as shown in Fig. 1 (b). The choice of the qudit is arbitrary due to the periodic boundary conditions. To quantify the information remained in the system in the presence of quantum noises with size-dependent probabilities, we measure the mutual information  $I_{AB:R} = S_{AB} + S_R - S_{AB \cup R}$  between the system and the reference qudit. To compare the results of the entanglement phase transition and the coding transition, we set their evolution times  $T$  to be equal.

*Statistical model.*— Here, we present the analytical understanding of these noise-induced phase transitions and the theoretical predictions of the critical behaviors. We focus on the discussions of mutual information for simplicity. Please refer to Refs. [55, 56] for more details of

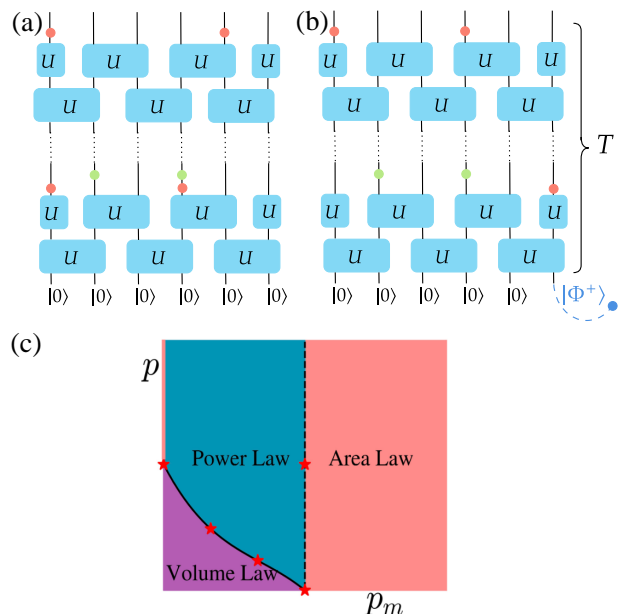


FIG. 1. Circuit setups with 6 qudits for (a) entanglement phase transition and (b) coding transition. The red and green circles represent the quantum channels and projective measurements, respectively. In (b), a qudit is maximally entangled with a reference qudit to encode one qudit information. (c) Phase diagram of entanglement phase transition with  $T = 4L$ . Red stars represent the critical points identified from numerical results. The solid (dashed) curve denotes the noise (measurement)-induced phase transition.

the effective statistical model and the perspective of logarithmic entanglement negativity.

Via a mapping from the hybrid quantum circuit to an effective statistical model by averaging over the Haar random two-qudit unitary gates, the entanglement entropy can be obtained from the free energy of a classical ferromagnetic spin model with particular top boundary conditions [55, 56]. The random space-time locations of projective measurements and quantum noises remain as quenched disorders on top of the spin model. In the large  $d$  limit, the free energy and thus the entanglement entropy of the hybrid circuits are determined by the dominant spin configuration with the largest weight.

In the classical spin model corresponding to  $S_{AB}$ , the top boundary condition is fixed to  $\mathbb{C}$  while the quantum noises act as magnetic fields pinning the classical spins in the  $\mathbb{I}$  direction. The weight of the spin configuration where all spins are fixed to  $\mathbb{C}$  as shown in Fig. 2 (a) is  $d^{-|\mathbb{C}|qLT}$ , where  $|\mathbb{C}|$  represents the unit energy and  $qLT$  is the average number of quantum noises. Therefore, the free energy of this spin configuration is proportional to  $qLT$ . However, this spin configuration is not favored compared to the spin configuration with a domain wall between the top and bottom boundaries as shown in Fig. 2 (b) when the scaling exponent of the quantum noises

is  $\alpha = 0.0$ . The free energy of the latter spin configuration with a domain wall when  $0 < p_m < p_m^c$  can be obtained using the KPZ theory with the leading order proportional to the domain wall length as  $s_0 L$ . Therefore, when the scaling exponent is  $\alpha = 1.0$ , there is a competition between these two spin configurations. It is worth noting that a spin configuration with a domain wall is always favored for the classical spin model corresponding to  $S_{A(B)}$  due to the fixed top boundary conditions and thus the leading term of free energy of  $S_A + S_B$  is  $s_0 L$ . When the probability  $p < s_0 L/T$ , the spin configuration with all spins fixed to  $\mathbb{C}$  is dominant and the mutual information is proportional to  $(s_0 - p)L$ , following a volume law. On the other hand, when the probability  $p > s_0 L/T$ , the leading terms cancel out and the mutual information is determined by the boundary term of the entanglement entropy, which follows a power law, specifically  $I_{A:B} \sim (L/p)^{1/3}$  [55, 56].

Notably, this is a first-order phase transition arising from the competition of different spin configurations. Furthermore, the spin configuration with all spins fixed to  $\mathbb{C}$  always dominates with the scaling exponent  $\alpha > 1.0$  (volume-law entanglement), while the spin configuration with the creation of a domain wall is always favored with the scaling exponent  $\alpha < 1.0$  (power-law entanglement). Therefore, this noise-induced phase transition only occurs with scaling exponent  $\alpha = 1.0$ . Though with the same exponent  $\alpha = 1$ , it is worth noting that the boundary quantum noise is relevant for the power law phase, and no phase transition between the volume law phase and the power law phase [57].

Next, we consider the noise-induced coding transition. In addition to the particular top boundary conditions discussed above, the spin at the bottom corresponding to the Bell pair is fixed by the top boundary conditions of the reference qubit:  $\mathbb{I}, \mathbb{C}, \mathbb{C}$  for  $S_{AB}, S_R$  and  $S_{AB \cup R}$ , respectively, see Fig. 2 (c) and (d).  $S_R$  remains constant because the dominant spin configuration is that all spins are  $\mathbb{I}$ , regardless of the probability of quantum noises. Therefore, the free energy is determined by the defect created at the bottom due to the Bell pair. However, for  $S_{AB}$  and  $S_{AB \cup R}$ , there is also a competition between the spin configuration with all spins fixed to  $\mathbb{C}$  and the spin configuration with a domain wall between the top and bottom boundaries, as shown in Fig. 2 (c) and (d). As a result, a noise-induced coding transition occurs, and it should have the same critical probability and exponent as the entanglement phase transition from the perspective of the effective statistical model. In other words, the two phase transitions are unified via the lens of the effective statistical model.

*Numerical results.*— To validate our theoretical predictions, we conduct extensive simulations of large-scale stabilizer circuits where random Clifford two-qubit unitary gates form a unitary 3-design [84, 85] and thus give qualitatively similar entanglement behaviors as the Haar

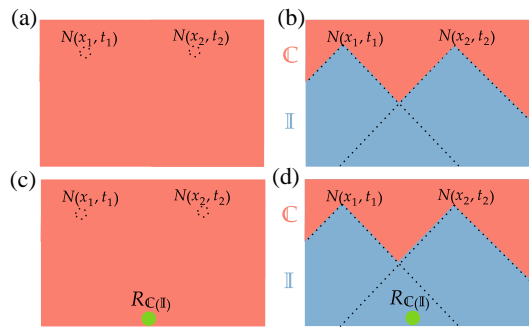


FIG. 2. The spin configurations of the effective statistical model. (a)(b) show the two competing spin configurations for  $S_{AB}$  in the entanglement phase transition. The effective length scale of the domain wall shown in (b) is determined by the average distance between adjacent quantum noises. In the presence of projective measurements, the domain wall will fluctuate away from its original path. (c)(d) show the two competing spin configurations in the coding transition. The spin corresponding to the Bell pair is denoted as  $R$  and is fixed to  $\mathbb{I}$  and  $\mathbb{C}$  for  $S_{AB}$  and  $S_{AB \cup R}$  respectively.  $N$  represents quantum noise and other quantum noises in the bulk are not shown here.

random gates. To model the quantum noise, we employed the reset channel defined as follows

$$\mathcal{R}_i(\rho) = \text{tr}_i(\rho) \otimes |0\rangle\langle 0|_i. \quad (3)$$

We note that the conclusions are independent of the choice of the quantum channels [56].

We set the scaling exponent of quantum noises  $\alpha = 1.0$  and the probability of measurements  $p_m < p_m^c$ . The numerical results of logarithmic entanglement negativity  $E_N$  and mutual information  $I_{A:B}$  in the presence of projective measurements with a fixed probability  $p_m = 0.2$  and quantum noises with varying probabilities are shown in Fig. 3 (a) and (b). The  $y$ -axis represents the rescaled entanglement within the system, denoted as  $E_N/L^{1/3}$  or  $I_{A:B}/L^{1/3}$ . In the power-law entanglement phase with large probabilities of quantum noises, the data obtained from different system sizes should collapse onto a single curve. Conversely, in the volume entanglement phase, the rescaled entanglement should increase as the system size increases. We observe a crossing point at a critical probability,  $p_c$ , indicating the noise-induced entanglement phase transition. To determine this critical probability, we employ data collapse with a scaling function

$$S(p, L)/L^{1/3} = F\left((p - p_c)L^{1/\nu}\right), \quad (4)$$

where  $S$  represents  $E_N$  or  $I_{A:B}$ ,  $\nu$  is the critical exponent that is fixed to 2.0 arising from the randomness of quantum noises [65]. The data collapse is shown in the insets of Fig. 3. Similarly, we show the  $I_{A:B} \sim (L/p)^{1/3}$  scaling as illustrated in Fig. 3 (c) and (d). Therefore, we have demonstrated the noise-induced entanglement

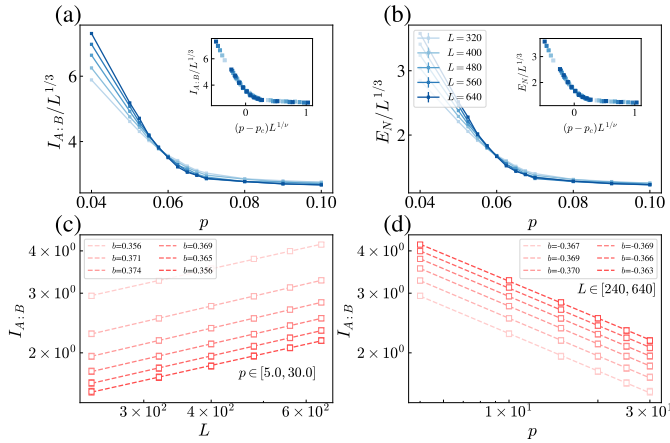


FIG. 3. The probability of reset channel is  $q = p/L$  and the probability of projective measurement is  $p_m = 0.2$ . We set  $T = 4L$ . (a) shows the rescaled mutual information within the system  $I_{A:B}/L^{1/3}$  vs noise probability  $p$ ; (b) shows the rescaled logarithmic negativity within the system  $E_N/L^{1/3}$  vs noise probability  $p$ . There is a noise-induced entanglement phase transition from a volume law phase to a power law phase with the increase of noise probability  $p$ . The insets show the data collapse with  $p_c = 0.0593$  and  $\nu = 2.0$ . (c)(d) show the fitting of the mutual information. The obtained power is very close to the theoretical predictions, showing that  $I_{A:B} \sim (L/p)^{1/3}$  in this noise-induced power law entanglement phase.

phase transition from a volume-law phase to a power-law phase numerically. Additional numerical results can be found in the Supplemental Material (SM) [86]. In the absence of projective measurements, there is an area-law entanglement phase instead of a power-law entanglement phase when the probability of quantum noise is large [86].

Next, we numerically investigate the noise-induced coding transition with the setup shown in Fig. 1 (b). The numerical results of mutual information  $I_{AB:R}$  between the system and the reference qubit are shown in Fig. 4 (a). When the quantum noises are sparse with a small probability, the encoded quantum information can be perfectly protected in the thermodynamic limit, i.e.,  $I_{AB:R} = 2.0$ . We note that the information is partially protected when the boundary noise probability is below the critical point, and a pre-scrambling process is necessary for perfect information protection [65]. Furthermore, in contrast to the setup shown in Fig. 1 (b), where the numerical results for finite  $d$  match well with the theoretical analysis from large  $d$  limit, when quantum noises occur at the spatial boundary and  $T/L < 1$ , the coding transition exists with finite  $d$  while it is absent in the large  $d$  limit due to the entropy contribution. The detailed discussions of the qualitative distinctions in the schematic phase diagram between these two setups can be found in the SM [86]. When  $p$  is large, the information is destroyed, and the mutual information  $I_{AB:R} = 0.0$ .

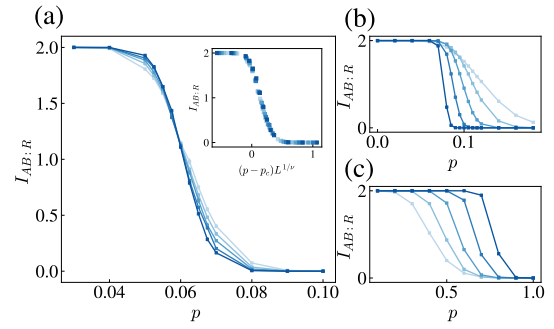


FIG. 4. (a) shows the noise-induced coding transition in the presence of quantum noises with scaling exponent  $\alpha = 1.0$ . The probability of projective measurement is  $p_m = 0.2$  and we set  $T = 4L$ . The inset shows the data collapse with critical probability  $p_c = 0.0543(73)$  and critical exponent  $\nu = 2.052(556)$  which are consistent with those of noise-induced entanglement phase transition. (b) shows the mutual information  $I_{AB:R}$  with scaling exponent  $\alpha = 0.8$  and (c) shows the mutual information  $I_{AB:R}$  with scaling exponent  $\alpha = 1.2$ . The noise-induced phase transitions disappear when scaling exponent  $\alpha \neq 1.0$ .

The inset of Fig. 4 (a) shows the data collapse, and we relax the constraint of the critical exponent. The obtained critical probability and exponent are consistent with those obtained from the noise-induced entanglement phase transition. See more numerical results in SM [86].

Furthermore, as discussed above, the scaling exponent  $\alpha = 1.0$  is crucial for these noise-induced phase transitions. Here, we show the numerical results of mutual information  $I_{AB:R}$  with scaling exponents  $\alpha = 0.8$  and  $\alpha = 1.2$  as shown in Fig. 4 (b) and (c) respectively. The encoded information will always be destroyed in the presence of quantum noises with scaling exponent  $\alpha < 1.0$  while the information will be perfectly protected in the presence of quantum noises with scaling exponent  $\alpha > 1.0$ , in the thermodynamic limit.

*Conclusions and discussion.*— We have investigated the noise-induced entanglement phase transition and coding transition in the presence of quantum noises with scaling exponent  $\alpha = 1.0$ . Theoretical analysis reveals that these phase transitions can be understood by the competition between different spin configurations within an effective statistical model. Through numerical simulations, we have identified these noise-induced phase transitions and critical behaviors. We have generalized the framework of MIPTs to the cases with quantum noises as shown in Fig. 1. Additionally, the influence of the scaling exponents has also been discussed. Moreover, we investigated the  $(L/p)^{1/2}$  timescale of information protection of the steady states, to further validate our theoretical analysis [56, 86].

Furthermore, we note that the noise-induced entanglement or coding transitions have a slightly different statistical model picture compared to the noise-induced

computational complexity transition in random circuit sampling [58–60]. In the latter case, there is no need to introduce replicas, and the critical probability  $p_c$  is independent of the choice of the ratio  $L/T$  which is analytically predicted as  $p_c \approx 1$ . However, for noise-induced entanglement or coding transitions discussed in this Letter,  $p_c \sim L/T$ . If  $L/T \rightarrow 0$ , these noise-induced phase transitions vanish, which is consistent with the fact that the encoded information is ultimately destroyed in the presence of quantum noises. To demonstrate these differences, we have conducted simulations to investigate noise-induced computational complexity transition in Clifford circuits. The obtained critical probability  $p_c$  is close to the theoretical prediction 1.0 [60] and the critical exponent is  $\nu \approx 1.0$ . See more numerical results and discussions in the SM [86].

*Acknowledgement.*— This work is supported in part by the NSFC under Grant No. 11825404 and 12334003 (SL, MRL, and HY), and by the MOSTC under Grant No. 2021YFA1400100 (HY). SL and MRL acknowledge the support from the Lavin-Bernick Grant during the visit to Tulane University. The work of SKJ is supported by a startup fund at Tulane University.

---

\* shixinzhang@tencent.com

† sjian@tulane.edu

‡ yaohong@tsinghua.edu.cn

- [1] Y. Li, X. Chen, and M. P. A. Fisher, Quantum zeno effect and the many-body entanglement transition, *Phys. Rev. B* **98**, 205136 (2018).
- [2] Y. Li, X. Chen, and M. P. A. Fisher, Measurement-driven entanglement transition in hybrid quantum circuits, *Phys. Rev. B* **100**, 134306 (2019).
- [3] B. Skinner, J. Ruhman, and A. Nahum, Measurement-induced phase transitions in the dynamics of entanglement, *Phys. Rev. X* **9**, 031009 (2019).
- [4] M. Ippoliti and V. Khemani, Postselection-free entanglement dynamics via spacetime duality, *Phys. Rev. Lett.* **126**, 060501 (2021).
- [5] T.-C. Lu and T. Grover, Spacetime duality between localization transitions and measurement-induced transitions, *PRX Quantum* **2**, 040319 (2021).
- [6] M. Ippoliti, T. Rakovszky, and V. Khemani, Fractal, logarithmic, and volume-law entangled nonthermal steady states via spacetime duality, *Phys. Rev. X* **12**, 011045 (2022).
- [7] M. J. Gullans and D. A. Huse, Dynamical purification phase transition induced by quantum measurements, *Phys. Rev. X* **10**, 041020 (2020).
- [8] S. Choi, Y. Bao, X.-L. Qi, and E. Altman, Quantum error correction in scrambling dynamics and measurement-induced phase transition, *Phys. Rev. Lett.* **125**, 030505 (2020).
- [9] A. Chan, R. M. Nandkishore, M. Pretko, and G. Smith, Unitary-projective entanglement dynamics, *Phys. Rev. B* **99**, 224307 (2019).
- [10] M. Szyniszewski, A. Romito, and H. Schomerus, Entanglement transition from variable-strength weak measurements, *Phys. Rev. B* **100**, 064204 (2019).
- [11] Y. Bao, S. Choi, and E. Altman, Theory of the phase transition in random unitary circuits with measurements, *Phys. Rev. B* **101**, 104301 (2020).
- [12] R. Fan, S. Vijay, A. Vishwanath, and Y.-Z. You, Self-organized error correction in random unitary circuits with measurement, *Phys. Rev. B* **103**, 174309 (2021).
- [13] Y. Li and M. P. A. Fisher, Statistical mechanics of quantum error correcting codes, *Phys. Rev. B* **103**, 104306 (2021).
- [14] C.-M. Jian, Y.-Z. You, R. Vasseur, and A. W. W. Ludwig, Measurement-induced criticality in random quantum circuits, *Phys. Rev. B* **101**, 104302 (2020).
- [15] E. V. H. Doggen, Y. Gefen, I. V. Gornyi, A. D. Mirlin, and D. G. Polyakov, Evolution of many-body systems under ancilla quantum measurements, *Phys. Rev. B* **107**, 214203 (2023).
- [16] J. C. Hoke, M. Ippoliti, E. Rosenberg, D. Abanin, R. Acharya, T. I. Andersen, M. Ansmann, F. Arute, K. Arya, A. Asfaw, J. Atalaya, J. C. Bardin, A. Bengtsson, G. Bortoli, A. Bourassa, J. Bovaird, L. Brill, M. Broughton, B. B. Buckley, D. A. Buell, T. Burger, B. Burkett, N. Bushnell, Z. Chen, B. Chiaro, D. Chik, J. Cogan, R. Collins, P. Conner, W. Courtney, A. L. Crook, B. Curtin, A. G. Dau, D. M. Debroy, A. Del Toro Barba, S. Demura, A. Di Paolo, I. K. Drozdov, A. Dunsworth, D. Eppens, C. Erickson, E. Farhi, R. Fatemi, V. S. Ferreira, L. F. Burgos, E. Forati, A. G. Fowler, B. Foxen, W. Giang, C. Gidney, D. Gilboa, M. Giustina, R. Gosula, J. A. Gross, S. Habegger, M. C. Hamilton, M. Hansen, M. P. Harrigan, S. D. Harrington, P. Heu, M. R. Hoffmann, S. Hong, T. Huang, A. Huff, W. J. Huggins, S. V. Isakov, J. Iveland, E. Jeffrey, Z. Jiang, C. Jones, P. Juhas, D. Kafri, K. Kechedzhi, T. Khattar, M. Khezri, M. Kieferová, S. Kim, A. Kitaev, P. V. Klimov, A. R. Klots, A. N. Korotkov, F. Kostritsa, J. M. Kreikebaum, D. Landhuis, P. Laptev, K.-M. Lau, L. Laws, J. Lee, K. W. Lee, Y. D. Lensky, B. J. Lester, A. T. Lill, W. Liu, A. Locharla, O. Martin, J. R. McClean, M. McEwen, K. C. Miao, A. Mieszala, S. Montazeri, A. Morvan, R. Movassagh, W. Mruczkiewicz, M. Neeley, C. Neill, A. Nersisyan, M. Newman, J. H. Ng, A. Nguyen, M. Nguyen, M. Y. Niu, T. E. O’Brien, S. Omonije, A. Opremcak, A. Petukhov, R. Potter, L. P. Pryadko, C. Quintana, C. Rocque, N. C. Rubin, N. Saei, D. Sank, K. Sankaragomathi, K. J. Satzinger, H. F. Schurkus, C. Schuster, M. J. Shearn, A. Shorter, N. Shutty, V. Shvarts, J. Skrzynny, W. C. Smith, R. Somma, G. Sterling, D. Strain, M. Szalay, A. Torres, G. Vidal, B. Villalonga, C. V. Heidweiller, T. White, B. W. K. Woo, C. Xing, Z. J. Yao, P. Yeh, J. Yoo, G. Young, A. Zalcman, Y. Zhang, N. Zhu, N. Zobrist, H. Neven, R. Babbush, D. Bacon, S. Boixo, J. Hilton, E. Lucero, A. Megrant, J. Kelly, Y. Chen, V. Smelyanskiy, X. Mi, V. Khemani, P. Roushan, and Google Quantum AI and Collaborators, Measurement-induced entanglement and teleportation on a noisy quantum processor, *Nature* **622**, 481 (2023).
- [17] Z.-C. Yang, Y. Li, M. P. A. Fisher, and X. Chen, Entanglement phase transitions in random stabilizer tensor networks, *Phys. Rev. B* **105**, 104306 (2022).
- [18] X. Turkeshi, R. Fazio, and M. Dalmonte, Measurement-induced criticality in (2+1)-dimensional hybrid quantum

- circuits, *Phys. Rev. B* **102**, 014315 (2020).
- [19] P. Sierant, M. Schirò, M. Lewenstein, and X. Turkeshi, Measurement-induced phase transitions in  $(d + 1)$ -dimensional stabilizer circuits, *Phys. Rev. B* **106**, 214316 (2022).
- [20] H. Liu, T. Zhou, and X. Chen, Measurement-induced entanglement transition in a two-dimensional shallow circuit, *Phys. Rev. B* **106**, 144311 (2022).
- [21] X. Feng, B. Skinner, and A. Nahum, Measurement-induced phase transitions on dynamical quantum trees, *PRX Quantum* **4**, 030333 (2023).
- [22] U. Agrawal, A. Zabalo, K. Chen, J. H. Wilson, A. C. Potter, J. H. Pixley, S. Gopalakrishnan, and R. Vasseur, Entanglement and charge-sharpening transitions in  $u(1)$  symmetric monitored quantum circuits, *Phys. Rev. X* **12**, 041002 (2022).
- [23] H. Oshima and Y. Fuji, Charge fluctuation and charge-resolved entanglement in a monitored quantum circuit with  $u(1)$  symmetry, *Phys. Rev. B* **107**, 014308 (2023).
- [24] F. Barratt, U. Agrawal, S. Gopalakrishnan, D. A. Huse, R. Vasseur, and A. C. Potter, Field theory of charge sharpening in symmetric monitored quantum circuits, *Phys. Rev. Lett.* **129**, 120604 (2022).
- [25] Y. Han and X. Chen, Entanglement dynamics in  $u(1)$  symmetric hybrid quantum automaton circuits, *arXiv:2305.18141* (2023).
- [26] S.-K. Jian, C. Liu, X. Chen, B. Swingle, and P. Zhang, Measurement-induced phase transition in the monitored sachdev-ye-kitaev model, *Phys. Rev. Lett.* **127**, 140601 (2021).
- [27] S. Sahu, S.-K. Jian, G. Bentsen, and B. Swingle, Entanglement phases in large- $n$  hybrid brownian circuits with long-range couplings, *Phys. Rev. B* **106**, 224305 (2022).
- [28] S.-K. Jian and B. Swingle, Phase transition in von Neumann entanglement entropy from replica symmetry breaking, *arXiv:2108.11973* (2021).
- [29] X. Yu and X.-L. Qi, Measurement-Induced Entanglement Phase Transition in Random Bilocal Circuits, *arXiv:2201.12704* (2022).
- [30] A. Nahum, S. Roy, B. Skinner, and J. Ruhman, Measurement and entanglement phase transitions in all-to-all quantum circuits, on quantum trees, and in landau-ginsburg theory, *PRX Quantum* **2**, 010352 (2021).
- [31] P. Sierant, G. Chiriaco, F. M. Surace, S. Sharma, X. Turkeshi, M. Dalmonte, R. Fazio, and G. Pagano, Dissipative Floquet Dynamics: from Steady State to Measurement Induced Criticality in Trapped-ion Chains, *Quantum* **6**, 638 (2022).
- [32] G. S. Bentsen, S. Sahu, and B. Swingle, Measurement-induced purification in large- $n$  hybrid brownian circuits, *Phys. Rev. B* **104**, 094304 (2021).
- [33] T. Müller, S. Diehl, and M. Buchhold, Measurement-induced dark state phase transitions in long-ranged fermion systems, *Phys. Rev. Lett.* **128**, 010605 (2022).
- [34] M. Block, Y. Bao, S. Choi, E. Altman, and N. Y. Yao, Measurement-induced transition in long-range interacting quantum circuits, *Phys. Rev. Lett.* **128**, 010604 (2022).
- [35] T. Hashizume, G. Bentsen, and A. J. Daley, Measurement-induced phase transitions in sparse nonlocal scramblers, *Phys. Rev. Res.* **4**, 013174 (2022).
- [36] T. Minato, K. Sugimoto, T. Kuwahara, and K. Saito, Fate of measurement-induced phase transition in long-range interactions, *Phys. Rev. Lett.* **128**, 010603 (2022).
- [37] S. Sharma, X. Turkeshi, R. Fazio, and M. Dalmonte, Measurement-induced criticality in extended and long-range unitary circuits, *SciPost Phys. Core* **5**, 023 (2022).
- [38] P. Zhang, C. Liu, S.-K. Jian, and X. Chen, Universal Entanglement Transitions of Free Fermions with Long-range Non-unitary Dynamics, *Quantum* **6**, 723 (2022).
- [39] V. Ravindranath, Y. Han, Z.-C. Yang, and X. Chen, Entanglement steering in adaptive circuits with feedback, *Phys. Rev. B* **108**, L041103 (2023).
- [40] V. Ravindranath, Z.-C. Yang, and X. Chen, Free fermions under adaptive quantum dynamics, *arXiv:2306.16595* (2023).
- [41] N. O’Dea, A. Morningstar, S. Gopalakrishnan, and V. Khemani, Entanglement and absorbing-state transitions in interactive quantum dynamics, *arXiv:2211.12526* (2022).
- [42] P. Sierant and X. Turkeshi, Controlling entanglement at absorbing state phase transitions in random circuits, *Phys. Rev. Lett.* **130**, 120402 (2023).
- [43] S. Majidy, U. Agrawal, S. Gopalakrishnan, A. C. Potter, R. Vasseur, and N. Y. Halpern, Critical phase and spin sharpening in  $su(2)$ -symmetric monitored quantum circuits, *Phys. Rev. B* **108**, 054307 (2023).
- [44] A. Biella and M. Schirò, Many-body quantum zeno effect and measurement-induced subradiance transition, *Quantum* **5**, 528 (2021).
- [45] X. Turkeshi, A. Biella, R. Fazio, M. Dalmonte, and M. Schirò, Measurement-induced entanglement transitions in the quantum ising chain: From infinite to zero clicks, *Phys. Rev. B* **103**, 224210 (2021).
- [46] X. Turkeshi, M. Dalmonte, R. Fazio, and M. Schirò, Entanglement transitions from stochastic resetting of non-hermitian quasiparticles, *Phys. Rev. B* **105**, L241114 (2022).
- [47] M. Ippoliti and V. Khemani, Learnability transitions in monitored quantum dynamics via eavesdropper’s classical shadows, *arXiv:2307.15011* (2023).
- [48] A. A. Akhtar, H.-Y. Hu, and Y.-Z. You, Measurement-induced criticality is tomographically optimal, *arXiv:2308.01653* (2023).
- [49] A. G. Moghaddam, K. Pöyhönen, and T. Ojanen, Exponential shortcut to measurement-induced entanglement phase transitions, *Phys. Rev. Lett.* **131**, 020401 (2023).
- [50] Y. Bao, S. Choi, and E. Altman, Symmetry enriched phases of quantum circuits, *Annals of Physics* **435**, 168618 (2021).
- [51] B. C. Dias, D. Perkovic, M. Haque, P. Ribeiro, and P. A. McClarty, Quantum Noise as a Symmetry-Breaking Field, *arXiv:2208.13861* (2022).
- [52] S.-K. Jian, C. Liu, X. Chen, B. Swingle, and P. Zhang, Quantum error as an emergent magnetic field, *arXiv:2106.09635* (2021).
- [53] Y. Li and M. Claassen, Statistical mechanics of monitored dissipative random circuits, *Phys. Rev. B* **108**, 104310 (2023).
- [54] Z. Li, S. Sang, and T. H. Hsieh, Entanglement dynamics of noisy random circuits, *Phys. Rev. B* **107**, 014307 (2023).
- [55] S. Liu, M.-R. Li, S.-X. Zhang, S.-K. Jian, and H. Yao, Universal kardar-parisi-zhang scaling in noisy hybrid quantum circuits, *Phys. Rev. B* **107**, L201113 (2023).
- [56] S. Liu, M.-R. Li, S.-X. Zhang, and S.-K. Jian, Entanglement structure and information protection in noisy hybrid quantum circuits, *arXiv:2401.01593* (2024).

- [57] Z. Weinstein, Y. Bao, and E. Altman, Measurement-induced power-law negativity in an open monitored quantum circuit, *Phys. Rev. Lett.* **129**, 080501 (2022).
- [58] A. Morvan, B. Villalonga, X. Mi, S. Mandrà, A. Bengtsson, P. Klimov, Z. Chen, S. Hong, C. Erickson, I. Drozdov, *et al.*, Phase transition in random circuit sampling, [arXiv:2304.11119](https://arxiv.org/abs/2304.11119) (2023).
- [59] B. Ware, A. Deshpande, D. Hangleiter, P. Niroula, B. Fefferman, A. V. Gorshkov, and M. J. Gullans, A sharp phase transition in linear cross-entropy benchmarking, [arXiv:2305.04954](https://arxiv.org/abs/2305.04954) (2023).
- [60] S. Sahu and S.-K. Jian, Phase transitions in sampling and error correction in local brownian circuits, [arXiv:2307.04267](https://arxiv.org/abs/2307.04267) (2023).
- [61] H. Kim and D. A. Huse, Ballistic spreading of entanglement in a diffusive nonintegrable system, *Phys. Rev. Lett.* **111**, 127205 (2013).
- [62] A. Nahum, J. Ruhman, S. Vijay, and J. Haah, Quantum entanglement growth under random unitary dynamics, *Phys. Rev. X* **7**, 031016 (2017).
- [63] M. Ippoliti, M. J. Gullans, S. Gopalakrishnan, D. A. Huse, and V. Khemani, Entanglement phase transitions in measurement-only dynamics, *Phys. Rev. X* **11**, 011030 (2021).
- [64] C. Noel, P. Niroula, D. Zhu, A. Risinger, L. Egan, D. Biswas, M. Cetina, A. V. Gorshkov, M. J. Gullans, D. A. Huse, and C. Monroe, Measurement-induced quantum phases realized in a trapped-ion quantum computer, *Nature Physics* **18**, 760 (2022).
- [65] I. Lovas, U. Agrawal, and S. Vijay, Quantum coding transitions in the presence of boundary dissipation, [arXiv:2304.02664](https://arxiv.org/abs/2304.02664) (2023).
- [66] M. Kardar, G. Parisi, and Y.-C. Zhang, Dynamic scaling of growing interfaces, *Phys. Rev. Lett.* **56**, 889 (1986).
- [67] M. Kardar, Roughening by impurities at finite temperatures, *Phys. Rev. Lett.* **55**, 2923 (1985).
- [68] D. A. Huse, C. L. Henley, and D. S. Fisher, Huse, henley, and fisher respond, *Phys. Rev. Lett.* **55**, 2924 (1985).
- [69] E. Medina, T. Hwa, M. Kardar, and Y.-C. Zhang, Burgers equation with correlated noise: Renormalization-group analysis and applications to directed polymers and interface growth, *Phys. Rev. A* **39**, 3053 (1989).
- [70] T. Gueudré and P. L. Doussal, Directed polymer near a hard wall and kpz equation in the half-space, *Europhysics Letters* **100**, 26006 (2012).
- [71] G. Barraquand, A. Krajenbrink, and P. Le Doussal, Half-Space Stationary Kardar–Parisi–Zhang Equation, *Journal of Statistical Physics* **181**, 1149 (2020).
- [72] C. H. Bennett, D. P. DiVincenzo, J. A. Smolin, and W. K. Wootters, Mixed-state entanglement and quantum error correction, *Phys. Rev. A* **54**, 3824 (1996).
- [73] M. Horodecki, P. Horodecki, and R. Horodecki, Mixed-state entanglement and distillation: Is there a “bound” entanglement in nature?, *Phys. Rev. Lett.* **80**, 5239 (1998).
- [74] G. Vidal and R. F. Werner, Computable measure of entanglement, *Phys. Rev. A* **65**, 032314 (2002).
- [75] M. B. Plenio, Logarithmic negativity: A full entanglement monotone that is not convex, *Phys. Rev. Lett.* **95**, 090503 (2005).
- [76] P. Calabrese, J. Cardy, and E. Tonni, Entanglement negativity in quantum field theory, *Phys. Rev. Lett.* **109**, 130502 (2012).
- [77] P. Calabrese, J. Cardy, and E. Tonni, Entanglement negativity in extended systems: a field theoretical approach, *Journal of Statistical Mechanics: Theory and Experiment* **2013**, P02008 (2013).
- [78] T.-C. Lu and T. Grover, Singularity in entanglement negativity across finite-temperature phase transitions, *Phys. Rev. B* **99**, 075157 (2019).
- [79] T.-C. Lu, T. H. Hsieh, and T. Grover, Detecting topological order at finite temperature using entanglement negativity, *Phys. Rev. Lett.* **125**, 116801 (2020).
- [80] T.-C. Lu and T. Grover, Entanglement transitions as a probe of quasiparticles and quantum thermalization, *Phys. Rev. B* **102**, 235110 (2020).
- [81] K.-H. Wu, T.-C. Lu, C.-M. Chung, Y.-J. Kao, and T. Grover, Entanglement renyi negativity across a finite temperature transition: A monte carlo study, *Phys. Rev. Lett.* **125**, 140603 (2020).
- [82] S. Sang, Y. Li, T. Zhou, X. Chen, T. H. Hsieh, and M. P. Fisher, Entanglement negativity at measurement-induced criticality, *PRX Quantum* **2**, 030313 (2021).
- [83] H. Shapourian, S. Liu, J. Kudler-Flam, and A. Vishwanath, Entanglement negativity spectrum of random mixed states: A diagrammatic approach, *PRX Quantum* **2**, 030347 (2021).
- [84] Z. Webb, The Clifford group forms a unitary 3-design, [arXiv:1510.02769](https://arxiv.org/abs/1510.02769) (2016).
- [85] E. v. d. Berg, A simple method for sampling random Clifford operators, [arXiv:2008.06011](https://arxiv.org/abs/2008.06011) (2021).
- [86] See the Supplemental Material for more details.
- [87] P. Hayden and J. Preskill, Black holes as mirrors: quantum information in random subsystems, *Journal of High Energy Physics* **2007**, 120 (2007).

# Supplemental Material for “Noise-induced phase transitions in hybrid quantum circuits”

## CONTENTS

I. Distinction between bulk quantum noises and boundary quantum noises in the encoding transition	8
II. Noise-induced entanglement phase transition	9
III. Measurement-induced entanglement phase transition in the presence of quantum noises	11
IV. Noise-induced coding transition	11
V. Noise-induced complexity transition in random circuit sampling	11

### I. DISTINCTION BETWEEN BULK QUANTUM NOISES AND BOUNDARY QUANTUM NOISES IN THE ENCODING TRANSITION

In this section, we clarify the differences between the setup discussed in the main text with bulk quantum noises and the setup investigated in Ref. [65] with boundary quantum noises. The space-time distributions of quantum noises result in qualitative differences in information protection and the schematic phase diagram of the coding transition.

Firstly, we analyze the competition between different spin configurations in the large  $d$  limit to provide analytical predictions of the coding transition with quantum noises on the left boundary. Since  $S_R$  remains constant, we only consider the classical spin models corresponding to  $S_{AB}$  and  $S_{AB\cup R}$ . One possible spin configuration is that all spins are fixed to  $\mathbb{C}$  (see Fig. S1 (a) and (d)) resulting in a free energy (on average) of  $(qT + 1)|\mathbb{C}|$  and  $qT|\mathbb{C}|$  for  $S_{AB}$  and  $S_{AB\cup R}$  respectively. Consequently, the mutual information between the system and the reference qudit is  $I_{AB:R} = 2\log(d)$ , indicating that the encoded information is protected. On the other hand, when  $T/L < 1$ , another spin configuration is to create a domain wall that starts from the left boundary at time  $t_0$  and is annihilated at the bottom such that the Bell pair lives in the domain  $\mathbb{I}$  and the mutual information is zero. Thus, the quantum noises between 0 and  $t_0$  reside in the domain  $\mathbb{C}$  and other quantum noises reside in the domain  $\mathbb{I}$ , as shown in Fig. S1 (b). The free energy of this spin configuration is  $(qt_0 + (T - t_0))|\mathbb{C}|$ , which is larger than that of the former spin configuration. Therefore, the boundary noise-induced coding transition is absent in the large  $d$  limit. We note that the path of the domain wall with fixed  $t_0$  is not unique (see Fig. S1 (b)) and thus there is an entropy contribution to the free energy at finite temperature, i.e., finite  $d$ . Consequently, the boundary noise-induced coding transition with critical point  $q_c = 1 - O(d^{-2})$  occurs where the information is partially protected below the critical point [65]. When  $T/L > 1$ , another spin configuration is to create a domain wall that starts from the left-top corner and is annihilated by the right boundary with free energy  $L|\mathbb{C}|$ . The competition between this spin configuration and the spin configuration with all spins fixed to  $\mathbb{C}$  results in the first-order coding transition with critical point  $q_c \sim L/T$ . The schematic phase diagrams with infinite  $d$  and finite  $d$  are depicted in Fig. S2 (a) and (b) respectively. The presence of the pre-scrambling process [65] will not change the argument above in the large  $d$  limit.

For the setup considered in the main text, when the scaling exponent of quantum noise is  $\alpha = 1.0$ , i.e.,  $q = p/L$ , the free energy (on average) of the spin configuration with all spins fixed to  $\mathbb{C}$  is  $(pT + 1)|\mathbb{C}|$  and  $pT|\mathbb{C}|$  for  $S_{AB}$  and  $S_{AB\cup R}$  respectively. However, the free energy of the spin configuration with a domain wall is  $O(L|\mathbb{C}|)$  which does not depend on  $T_{\text{scr}}$  and ratio  $T/L$ . Consequently, even when  $T/L < 1.0$ , the noise-induced coding transition always exists and is independent of whether there is a pre-scrambling process. Moreover, below the critical point  $p_c \sim L/T$ , the information is perfectly protected even  $T_{\text{scr}} = 0$ . The numerical results are shown in Fig. S3. Furthermore, because of the unitary constraint, the dominant domain wall configuration is unique and large  $d$  limit analytical results can relate to the finite  $d$  numerical results. The schematic phase diagrams with infinite  $d$  and finite  $d$  are shown in Fig. S2 (c) and (d) respectively.

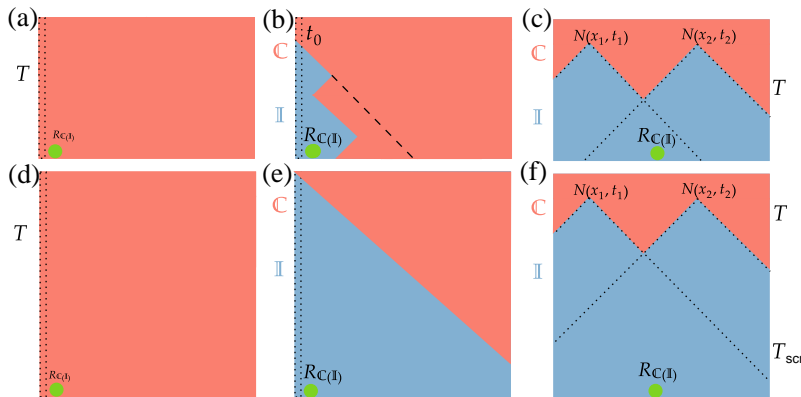


FIG. S1. (a) and (d) show the spin configurations with all spins fixed to  $\mathbb{C}$  with  $T/L < 1$  and  $T/L > 1$  respectively. (b) and (e) show the spin configurations with a domain wall. In (b), the black line shows another possible path for the domain wall with the same  $t_0$ . (c) and (f) show the domain wall configuration with quantum noises in the bulk without and with the scrambling process respectively.

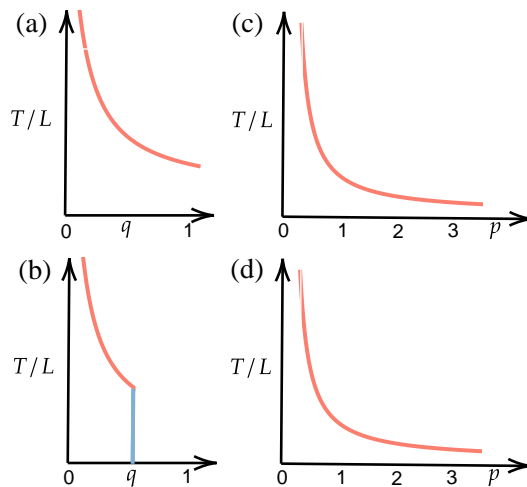


FIG. S2. Schematic phase diagrams for coding transition without pre-scrambling process. (a) left-boundary noises and  $d = \infty$ ; (b) left-boundary noises and  $d = 2$  [65]. (c) bulk noises and  $d = \infty$ ; (d) bulk noises and  $d = 2$ . In the presence of bulk quantum noises, the schematic phase diagrams are the same for  $d = 2$  and  $d = \infty$ . The red line represents a first-order transition while the blue line represents a continuous phase transition.

## II. NOISE-INDUCED ENTANGLEMENT PHASE TRANSITION

In this section, we present additional numerical results of the noise-induced entanglement phase transition. The numerical results for the mutual information and logarithmic entanglement negativity with fixed probability of measurements  $p_m = 0.1$  and  $T/L = 4$  are shown in Fig. S5. In the absence of projective measurements, the noise-induced entanglement phase transition still occurs. However, when the probability of noise  $p$  exceeds the critical value  $p_c$ , the entanglement within the system follows an area law, as illustrated in Fig. S6 and Fig. S8 (a). As discussed in the main text and the last section and shown in Fig. S3, the critical probability of noises will decrease with the ratio  $L/T$  decreases. Besides the phase diagram of entanglement phase transition with  $T/L = 4$  in the main text, we also show a schematic phase diagram with varying ratio  $L/T$  in Fig. S4. In the limit  $L/T \rightarrow 0$ , the noise-induced entanglement phase transition disappears, and the entanglement always obeys power law (area law) in the presence (absence) of projective measurements. From the perspective of coding transition, it is consistent with the fact that the encoded information is ultimately destroyed by the quantum noises.

Moreover, to validate our analytical understanding, we also investigate the timescale of information protection for

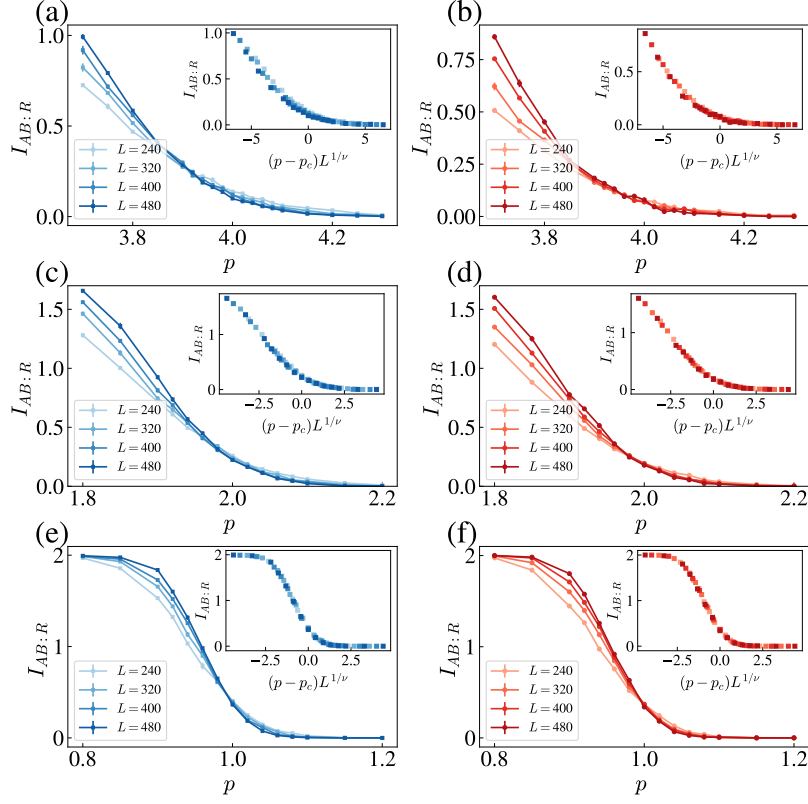


FIG. S3. The probability of reset channels is  $q = p/L$  and the probability of measurements is  $p_m = 0$ .  $T_{\text{scr}} = 0$  in the left panel and  $T_{\text{scr}} = L$  in the right panel. (a-b), (c-d), and (e-f) show the mutual information  $I_{AB:R}$  with  $T/L = 1/4, 1/2, 1$  respectively. Insets show the data collapse with  $p_c = L/T$  and  $\nu = 2.0$ .

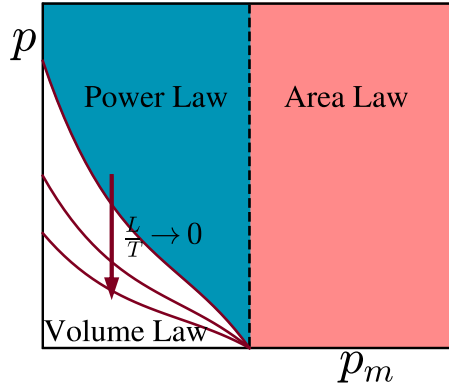


FIG. S4. Schematic phase diagram:  $p_c$  decreases with the ratio  $L/T$  decreases.

the steady states in this noise-induced power or area law entanglement phase. As discussed in our previous work [56], this timescale is  $q^{-1/2}$ , i.e.,  $(L/p)^{1/2}$  when  $p$  is much larger than  $p_c$  and can be understood as the analogy of the Hayden-Preskill protocol for black holes [87] in noisy hybrid quantum circuits. Consequently, the dynamics of mutual information  $I_{AB:R}$  can be collapsed with rescaled time  $t/(L/p)^{1/2}$ . The numerical results with  $p_m = 0.2$  and  $p_m = 0.0$  are shown in Fig. S7 and Fig. S8 (b) respectively.

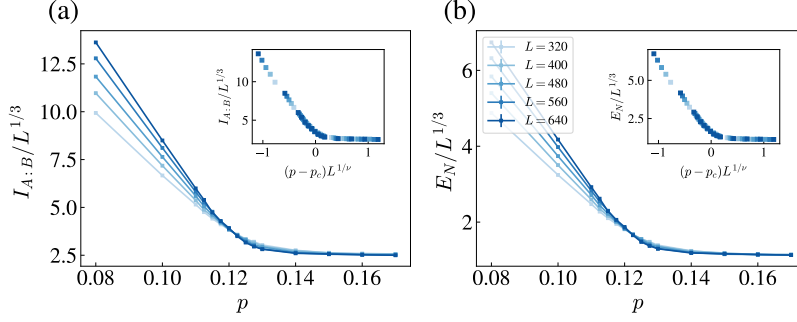


FIG. S5. The probability of reset channels is  $q = p/L$  and the probability of measurements is  $p_m = 0.1$ . We set  $T = 4L$ . (a) shows the rescaled mutual information within the system  $I_{A:B}/L^{1/3}$  vs noise probability  $p$ ; (b) shows the rescaled logarithmic negativity within the system  $E_N/L^{1/3}$  vs noise probability  $p$ . The insets show the data collapse with  $p_c = 0.123$  and  $\nu = 2.0$

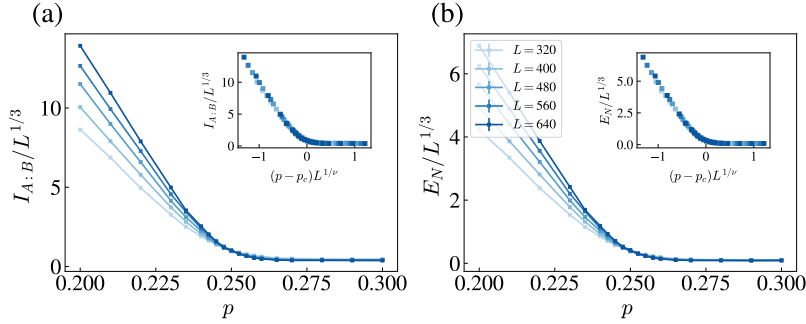


FIG. S6. The probability of reset channels is  $q = p/L$  and the probability of measurements is  $p_m = 0.0$ . We set  $T = 4L$ . (a) shows the rescaled mutual information within the system  $I_{A:B}/L^{1/3}$  vs noise probability  $p$ ; (b) shows the rescaled logarithmic negativity within the system  $E_N/L^{1/3}$  vs noise probability  $p$ . The insets show the data collapse with  $p_c = 0.252$  and  $\nu = 2.0$ .

### III. MEASUREMENT-INDUCED ENTANGLEMENT PHASE TRANSITION IN THE PRESENCE OF QUANTUM NOISES

In the section, we show more numerical results of measurement-induced entanglement phase transition in the presence of quantum noises with scaling exponent  $\alpha = 1.0$ . As shown in Fig. S9, there is a measurement-induced entanglement phase transition from power law to area law with the increases of measurement probabilities. The critical probability of measurements  $p_m^c$  and critical exponent  $\nu_m$  are consistent with those in MIPTs without quantum noises. We note that in the presence of quantum noises at spatial boundaries, the critical probability is also the same as that without quantum noises but the critical exponent changes which may be caused by the limited system sizes [57].

### IV. NOISE-INDUCED CODING TRANSITION

In this section, we present additional numerical results of the noise-induced coding transition. The numerical results of mutual information  $I_{AB:R}$  between the system ( $AB$ ) and the reference qubit  $R$  with measurement probabilities  $p_m = 0.1$  and  $p_m = 0.0$  are shown in Fig. S10 and Fig. S11 respectively. The critical exponent  $\nu$  is close to 2.0 and the critical probability  $p_c$  increases as the probability of measurements decreases.

### V. NOISE-INDUCED COMPLEXITY TRANSITION IN RANDOM CIRCUIT SAMPLING

In addition to the noise-induced entanglement and coding transitions, there is also a noise-induced computational complexity transition in random circuit sampling [58–60]. When the quantum noise is strong, the wavefunction of

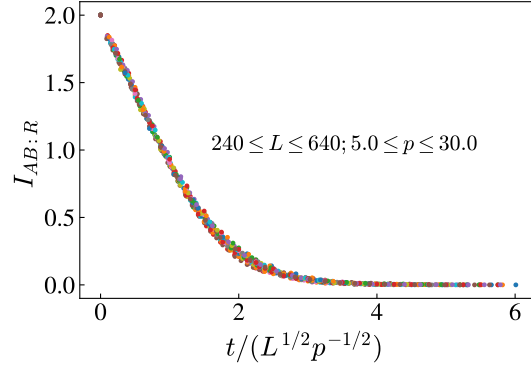


FIG. S7. The probability of reset channels is  $q = p/L$  and the probability of measurements is  $p_m = 0.2$ . The dynamics of mutual information  $I_{AB:R}$  can be collapsed with rescaled time  $t/(L/p)^{1/2}$ .

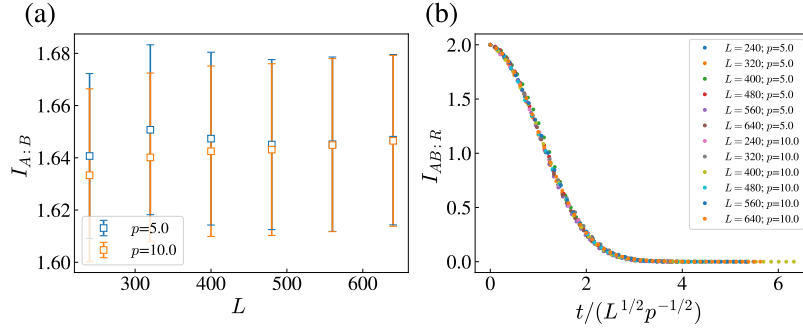


FIG. S8. The probability of reset channels is  $q = p/L$  and the probability of measurements is  $p_m = 0.0$ . (a) shows the mutual information  $I_{A:B}$  of the steady states vs system size  $L$  with the probability of noise  $p > p_c$ . The entanglement within the system obeys area law. (b) shows the dynamics of mutual information  $I_{AB:R}$  vs rescaled time  $t/(L/p)^{1/2}$ .

the system can be approximately represented by multiple uncorrelated subsystems. This makes the quantum system vulnerable to spoofing by classical algorithms that only represent a part of the system. However, when the quantum noise is sufficiently weak, correlations span the entire system restoring its computational complexity. We demonstrate this transition numerically by the crossing of the ratio of the fidelity and the linear cross-entropy benchmarking (XEB). The noise-induced computational complexity transition is illustrated in Fig. S12 with noise probability  $q = p/L$ . When  $\alpha \neq 1.0$ , this complexity transition also disappears, see Fig. S13 for more details.

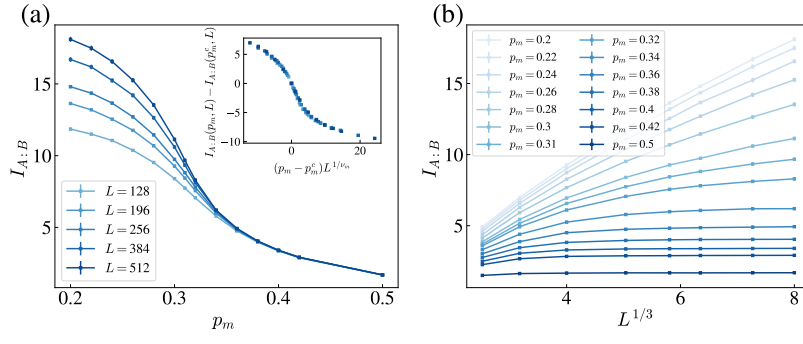


FIG. S9. The probability of reset channels is  $q = 0.252/L$  and  $T = 4L$ . (a)  $I_{A:B}$  vs  $p_m$ . Inset shows the data collapse with  $p_m = 0.3$  and  $\nu_m = 1.3$ . (b)  $I_{A:B}$  vs  $L^{1/3}$ . As the measurement probability increases, there is an entanglement phase transition from power law to area law.

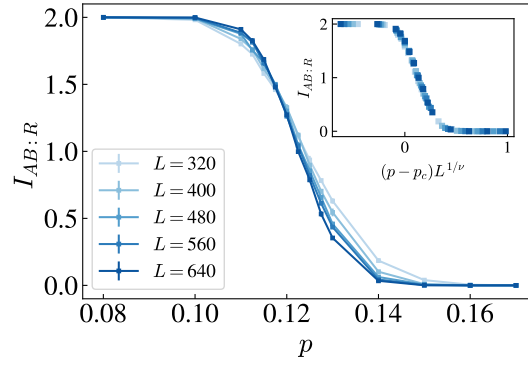


FIG. S10. The probability of reset channels is  $q = p/L$  and the probability of measurements is  $p_m = 0.1$ . We set  $T_{\text{scr}} = T$  and  $T = 4L$ . Inset shows the data collapse with  $p_c = 0.115(6)$  and  $\nu = 2.241(487)$ .

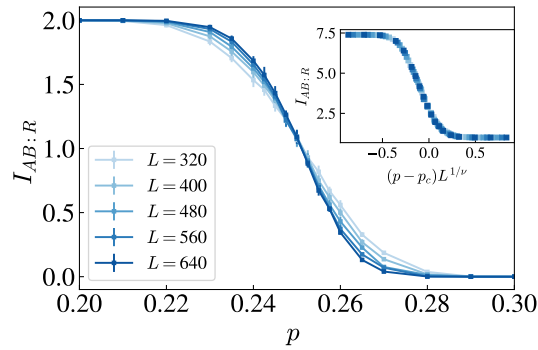


FIG. S11. The probability of reset channels is  $q = p/L$  and the probability of measurements is  $p_m = 0.0$ . We set  $T_{\text{scr}} = T$  and  $T = 4L$ . Inset shows the data collapse with  $p_c = 0.251(2)$  and  $\nu = 2.280(356)$ .

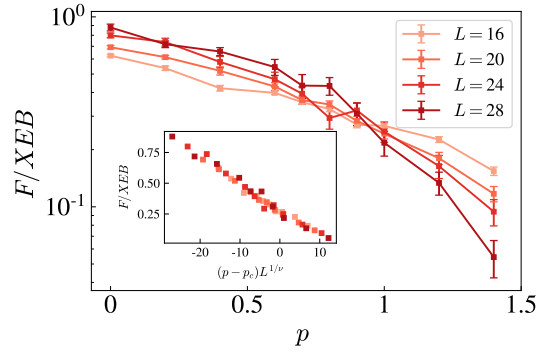


FIG. S12. The probability of quantum noises is  $q = p/L$ . The ratio of the fidelity and XEB vs noise probability  $p$ . There is a noise-induced complexity transition. The inset shows the data collapse with  $p_c \approx 0.96$  and  $\nu \approx 1$ .

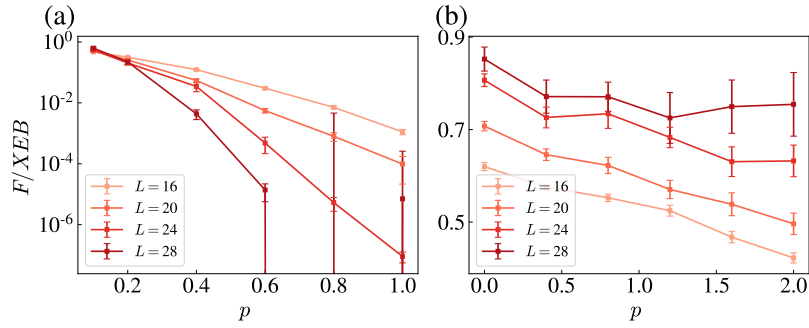


FIG. S13. Similar to cases of noise-induced entanglement and coding transitions, the complexity transition only exists with  $\alpha = 1.0$ . (a)(b) show the ratio of the fidelity and XEB vs noise probability  $p$  with scaling exponents  $\alpha = 0.5$  and  $\alpha = 1.5$ .